PAPER

Folate-receptor-targeted NIR-sensitive polydopamine nanoparticles for chemo-photothermal cancer therapy

To cite this article: Hao Li *et al* 2017 *Nanotechnology* **28** 425101

IOP Publishing Nanotechnology

Nanotechnology **28** (2017) 425101 (10pp) https://doi.org/10.1088/1361-6528/aa8477

Folate-receptor-targeted NIR-sensitive polydopamine nanoparticles for chemo-photothermal cancer therapy

Hao Li[1], Zhen Jin[1], Sunghoon Cho[1], Mi Jeong Jeon[1], Van Du Nguyen[1], Jong-Oh Park[1,3] and Sukho Park[1,2,3]

[1] School of Mechanical Engineering, Chonnam National University, 77 Yongbong-ro, Buk-gu, Gwangju, 61186, Republic of Korea
[2] Department of Robotics Engineering, Daegu Gyeongbuk Institute of Science and Technology, 333 Techno Jungang-daero, Hyeonpung-myeon, Dalseong-gun, Daegu, 42988, Republic of Korea

E-mail: jop@jnu.ac.kr and shpark12@dgist.ac.kr

Received 12 January 2017, revised 24 July 2017
Accepted for publication 7 August 2017
Published 25 September 2017

Abstract

We propose the use of folate-receptor-targeted, near-infrared-sensitive polydopamine nanoparticles (NPs) for chemo-photothermal cancer therapy as an enhanced type of drug-delivery system which can be synthesized by *in situ* polymerization and conjugation with folic acid. The NPs consist of a Fe_3O_4/Au core, coated polydopamine, conjugated folic acid, and loaded anti-cancer drug (doxorubicin). The proposed multifunctional NPs show many advantages for therapeutic applications such as good biocompatibility and easy bioconjugation. The polydopamine coating of the NPs show a higher photothermal effect and thus more effective cancer killing compared to Fe_3O_4/Au nanoparticles at the same intensity as near-infrared laser irradiation. In addition, the conjugation of folic acid was shown to enhance cancer cellular uptake efficiency via the folate receptor and thus improve chemotherapeutic efficiency. Through *in vitro* cancer cell treatment testing, the proposed multifunctional NPs showed advanced photothermal and chemotherapeutic performance. Based on these enhanced anti-cancer properties, we expect that the proposed multifunctional NPs can be used as a drug-delivery system in cancer therapy.

Supplementary material for this article is available online

Keywords: polydopamine, folic acid, chemo-photothermal therapy, polyfunctional nanoparticles, cancer therapy

(Some figures may appear in colour only in the online journal)

1. Introduction

Recently, external stimulus-responsive multifunctional nanoparticles (NPs) for remotely controllable cancer therapy have received more attention than existing cancer-therapeutic NPs. Since different materials can be assembled into a single nanostructure, NPs may have unprecedented properties and offer a promising method for achieving multiple functionalities derived from each building block [1–4]. Among the various multifunctional NPs, many researchers have focused on the synthesis and application of Au-coated magnetic iron NPs, as the coating not only endows them with unique magnetic and optical properties but also ensures their biocompatibility [5–9]. The benefits of the improved physical, chemical, and biological properties of multifunctional NPs may enable multimodal imaging [6], drug-delivery vehicles [9], and photothermal cancer therapy [4]. These types of drug-delivery systems could differentially increase drug accumulation at targeted lesions, decrease systemic toxicity and side effects, and enhance targeting accuracy [3, 4, 10–14].

[3] Authors to whom any correspondence should be addressed.

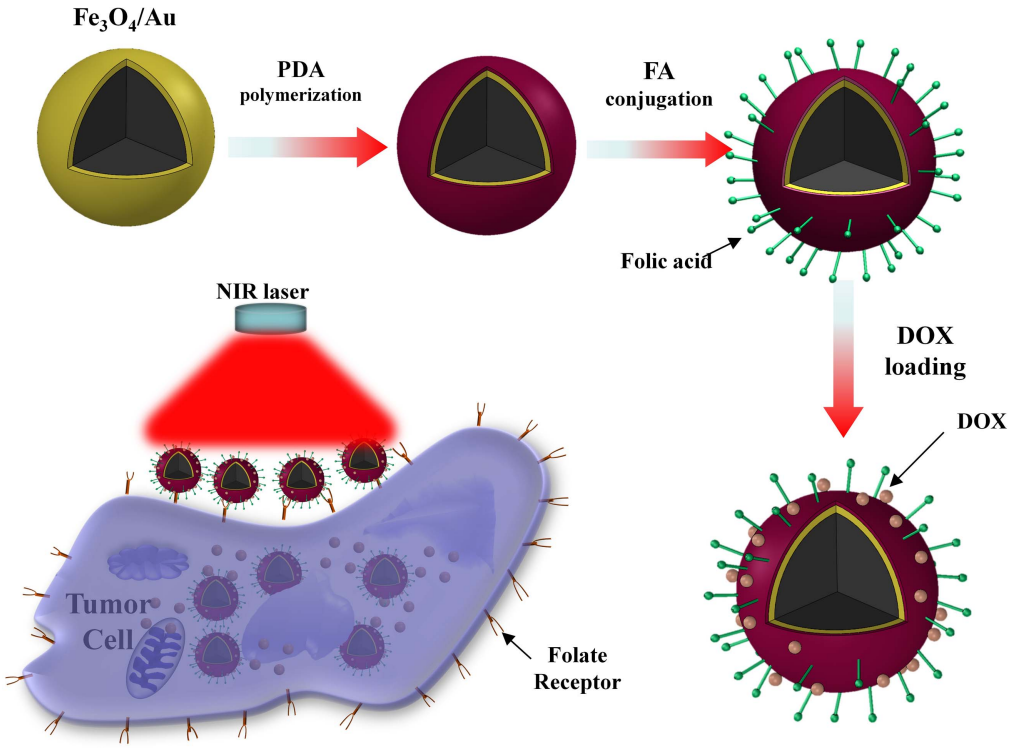

Figure 1. Schematic illustration of the fabrication of FR-targeted, NIR-sensitive polydopamine nanoparticle for chemo-photothermal cancer therapy. Fe_3O_4/Au was used as the metal core, dopamine was polymerized, and then the particle was conjugated with folic acid. The proposed drug-delivery system showed cell uptake efficiency and enhanced chemo-photothermal therapeutic efficiency.

Various external physical stimuli, including light, magnetic field, electric field, heat, ultrasound, and pH, have been used to enhance, trigger, or control localized cancer therapies [11, 15–19]. Among them, near infrared (NIR) light (605–900 nm) is regarded as attractive because of its easy operation and minimal absorbance by the skin and tissues to allow for noninvasive penetration of reasonably deep tissues. By employing different types of light-absorbing agents in NPs, NIR light can be effectively converted into heat in the accumulated NPs inside cancer cells [20]. In addition to hyperthermia resulting from the generated heat, NIR light can not only stimulate antineoplastic effects on cancer cells, but also increase the permeability of the cell membrane to improve intracellular drug uptake. These properties of NIR stimulus have a synergistic effect on cancer therapy compared with monotherapy [21].

There are many biocompatible NPs, such as gold and carbon nanomaterials, palladium nanosheets, polypyrrole, and copper sulfide, which are widely used as photothermal therapy (PTT) nano-agents [14, 22–25]. Many researchers have reported on various NPs combined with specific trigger methods for drug delivery in cancer therapy, and they have been regarded as emerging next-generation anticancer agents. However, there are still challenges in the development of multifunctional NPs with biocompatibility and no toxicity. Therefore, an enhanced drug-delivery system with both chemo- and photothermal therapeutic functions should be developed for potential drug delivery in cancer therapy. Recently, polydopamine (PDA) has been used as a photothermal therapeutic agent for cancer therapy because of its strong NIR absorption. Since PDA shows biodegradability and does not induce long-term toxicity during its retention in rats, it is superior to widely used metallic and carbon-based photothermal materials. Moreover, PDA provides a photothermal conversion of 40%—much higher than those of the previously reported PTT agents [26]. Finally, PDA can be easily attached to conjugates with other interesting biofunctionalities, which provides a particularly useful platform for simultaneous diagnoses and efficient treatment of cancer. There have been several reports describing the use of PDA as a photothermal agent of NPs, such as Fe_3O_4/PDA and melanin-PDA [27, 28]. However, in these studies, they used high intensities (about 1–5 W cm^{-2}) of NIR irradiation that could exceed the safe limit for cutaneous tissues (0.33 W cm^{-2}) [26]. For effective PTT treatments, therefore, the efficiency of energy conversion during PTT should be increased and the required laser dose should be reduced.

Various targeting moieties or ligands for tumor-cell-specific receptors have been immobilized on the surface of NPs to deliver them within tumor cells via receptor-mediated endocytosis [23, 29]. Among the diverse targeting ligands, folic acid (FA) has a low cost, is easily conjugated to NPs, and shows high stability during transportation, storage, and use [30]. Particularly, FA is a high-affinity ligand of folate receptors (FRs), which are frequently overexpressed in cancer cells, including those of ovary, brain, kidney, breast, colon, and lung cancers; however, its expression is low in normal tissues [29]. Therefore, FRs are good candidates for tumor-specific targeting in cancer therapy.

In this study, we propose FR-targeted, NIR-sensitive PDA NPs for chemo-photothermal cancer therapy (figure 1). Briefly, Fe_3O_4/Au was adopted as a metal core–shell structure that can be used for photothermal therapy and/or MRI imaging, and PDA was coated on the surface of the core–shell structure via the self-polymerization of dopamine powders for enhancing the photothermal cancer therapy. Next, FA was conjugated to the surface of the PDA-coated NPs and an anticancer drug (doxorubicin: DOX) was loaded. The proposed multifunctional NPs were characterized using transmission electron microscope (TEM), zeta-potential, Fourier transform infrared (FT-IR), thermogravimetric analysis (TGA), x-ray photoelectron spectroscopy (XPS), and vibrating sample magnetometer (VSM). We also evaluated the performance of NPs, including photothermal effects by NIR laser irradiation, cellular uptake efficiency by confocal laser scanning microscopy (CLSM), and controlled drug release using an NIR laser. Finally, the therapeutic effects of the proposed NPs for cancer cells were determined.

2. Materials and methods

2.1. Materials

Iron (III) chloride (reagent grade, 97%), iron (II) chloride (98%), branched polyethylenimine (PEI), gold (III) chloride trihydrate (⩾99.9% trace metals basis), hydroxylamine hydrochloride (99.999% trace metal basis), dopamine hydrochloride (DA), 1-ethyl-3(3-dimethylaminopropyl) carbodiimide hydrochloride (EDC), *N*-hydroxysuccinimide (NHS), and folic acid (FA) were purchased from Sigma-Aldrich (St. Louis, MO, USA). Sodium hydroxide (NaOH) was purchased from Junsei Chemical Co., Ltd (Toyko, Japan) and hydrochloric acid (HCl) was purchased from DUKSAN (Ansan-si, Korea). Additionally, doxorubicin (DOX) was supplied from Jinhe Bio-Technology (Shanghai, China). All chemicals were of analytical grade and used without further purification, and all aqueous solutions were prepared using ultrapure water from a Milli-Q system (Millipore, Billerica, MA, USA).

2.2. Preparation of highly monodispersed Fe_3O_4 NPs and Au-coated Fe_3O_4 NPs

Fe_3O_4 NPs were prepared using a standard co-precipitation technique in aqueous medium, as previously described [31]. Briefly, 10 mM iron (III) chloride and 5 mM iron (II) chloride were added to 12 ml hydrochloric acid (1 M) solution. This mixture was dissolved in 50 ml 1 M sodium solution in a four-neck round-bottom flask equipped with a mechanical stirrer. The reaction was performed in a non-oxidizing oxygen-free environment by bubbling N_2 in the reaction, which reduces the final size of the NPs, heated to 80 °C, and then maintained at that temperature for 2 h. The solution was then cooled to room temperature (25 °C), and the resulting particles were subjected to magnetic decantation followed by repeated washing with distilled water and ethanol. A portion of the resulting black precipitate was freeze-dried until use.

Next, 18 mg Fe_3O_4 powder was dissolved in 440 ml NaOH (0.01 M) solution and mechanically stirred with $NaH_2OH.HCl$ (0.2 M) and $HAuCl_4$ (1%, w/w) for five iterations [32]. In the first iteration, 0.5 ml of $HAuCl_4$ (1%) was added along with 0.25 ml of $NaH_2OH.HCl$ for 10 min. For the second iteration, 0.5 ml of $HAuCl_4$ (1%) and 0.75 ml of $NaH_2OH.HCl$ were added for 10 min. This latter procedure was repeated three more times, resulting in the final Fe_3O_4/Au NPs. Finally, we obtained Au-coated Fe_3O_4 (Fe_3O_4/Au) NPs.

2.3. Polydopamine coating and FA conjugation

First, for the polydopamine coating, 20 mg Fe_3O_4/Au was dispersed in 40 ml phosphate-buffered saline (PBS; pH 8.5) and ultrasonicated for 30 min. Next, 80 mg dopamine was added and the mixture was stirred for 24 h to obtain polydopamine-coated Fe_3O_4/Au. After washing with water three times, the PDA-coated Fe_3O_4/Au (Fe_3O_4/Au/PDA) NPs were collected by centrifugation at 5000 rpm for 10 min and washing with water three times. Finally, the PDA-coated Fe_3O_4/Au NPs were dispersed in water at a concentration of 5 mg ml^{-1} until further use.

Second, to conjugate with FA, 1 mg of Fe_3O_4/Au/PDA NPs were suspended in 200 μl of PEI (20 mg ml^{-1}) and stirred for 2 h to obtain PEI-functionalized Fe_3O_4/Au/PDA NPs. Next, 4 ml EDC (1 mg ml^{-1}) and 10 ml NHS (1 mg ml^{-1}) solutions were added to 1 ml FA solution (1 mg ml^{-1} in dimethyl sulfoxide) and reacted for 30 min to activate the carboxylic acid groups of FA. This solution was rapidly added into 1.0 ml PEI-functionalized Fe_3O_4/Au/PDA NP solution (1 mg ml^{-1}) and agitated for 12 h. Finally, the FA-conjugated Fe_3O_4/Au/PDA (Fe_3O_4/Au/PDA/PEI/FA) NPs were collected by centrifugation at 5000 rpm for 10 min and washed with water and ethanol. The obtained FA-conjugated Fe_3O_4/Au/PDA NPs were redispersed in pH 7.4 PBS and stored at 4 °C.

2.4. Drug loading and release

First, as a model anticancer drug, 20 mg DOX was added to 2.0 ml Fe_3O_4/Au/PDA/PEI/FA NPs (1 mg ml^{-1}) in PBS solution, and the mixture was shaken for 24 h in the dark at 37 °C. Next, DOX-loaded Fe_3O_4/Au/PDA/PEI/FA NPs (Fe_3O_4/Au/PDA/PEI/FA/DOX NPs) were separated from free DOX solution by centrifugation (12 000 rpm, 3 min). Next, we obtained the final Fe_3O_4/Au/PDA/PEI/FA/DOX NPs. To evaluate the drug-loading properties, the concentration of the remaining DOX solution was measured by a fluorescence spectrophotometer (λ_{ex} = 480 nm). The drug-loading efficiency was calculated as follows: encapsulation efficiency (%) = (fluorescence intensity of feed DOX-fluorescence intensity of DOX in solution)/(fluorescence intensity of feed DOX)) *100% [29]. The DOX encapsulation efficiency was found to be about 23.5%.

The drug-releasing test was performed using Fe_3O_4/Au/PDA/PEI/FA/DOX NPs in 1.0 ml of buffer solution at 37 °C. To determine the amount of drug released at any time, 1.0 ml of the solution was withdrawn after centrifugation and the same volume (1.0 ml) of buffer was added to keep the solution volume constant. The drug concentration in the withdrawn solution was analyzed by measuring the fluorescence intensity. This drug-release profiles were evaluated at least twice and cumulative drug release percentages as a function of time were recorded.

2.5. Cytotoxicity test

The cytotoxicity of the proposed NPs was determined by a 3-(4,5-dimethylthiazol-2yl)-2,5-diphenytetrazolium bromide (MTT) cell-proliferation assay [33]. Briefly, 4T1 breast cancer cells were seeded at a density of 10^4 cells per well in 96-well plates. The next day, the medium was replaced with different formulation solutions: fresh medium, Fe_3O_4/Au/PDA/PEI/FA/DOX NPs with DOX concentration (20 μg ml^{-1}) where the DOX concentration was directly determined by the corresponding NP concentration (100 μg ml^{-1}). After 12 h, the cell wells were placed in a live cell chamber at 37 °C and a certain group of wells was irradiated with an NIR laser for 5 min. After incubation for 12 h, the supernatants in the wells were removed, and then the cells were washed twice with PBS and incubated in Dulbecco's Modified Eagle's Medium containing MTT (5 mg ml^{-1}) for an additional 2 h. The MTT solutions were removed and dimethyl sulfoxide was added to dissolve the formazan crystals. The absorbance at 570 nm was measured by a microplate reader, and untreated cells were used as a negative control.

2.6. Characterization

FT-IR spectra were recorded on a Nicolet 6700 FT-IR spectrometer (Thermal Fisher, Waltham, MA, USA). TEM images were measured on a JEM-2100F Field Emission TEM (JEOL, Tokyo, Japan). CLSM studies were performed using a Leica TCS SP5 microscope (Mannheim, Germany) with excitation at 480 nm. Fluorescence spectra were obtained using a Shimadzu RF-5301PC spectrofluorophotometer (Kyoto, Japan). Zeta potential was tested on a micro-zeta potential analyzer (Malvern Instruments, Malvern, UK). TGA was performed using Shimadzu TGA-50 (Kyoto, Japan). XPS (Thermal Fisher, Waltham, MA, USA) was employed to acquire quantitative data on the structure of samples. MTT assay results were recorded at 570 nm using a Bio-Rad 680 microplate reader (Hercules, CA, USA). VSM was tested at room temperature using a 7404 VSM (Lake Shore Cryotronics, Westerville, OH, USA).

2.7. Experimental Setting

An important feature of Fe_3O_4/Au/PDA/PEI/FA/DOX NPs is the NIR light-induced thermal effect, which can be used for thermal-triggered drug release and hyperthermic treatment of solid tumors. To investigate the thermal effect, we used NIR light to irradiate Fe_3O_4/Au/PDA/PEI/FA/DOX NPs. For NIR light irradiation, we used a continuous-wave, fiber-coupled diode light (center wavelength: 808 nm) with an external adjustable power (CNI, New Industries Optoelectronics Tech. Co. Ltd, Changchun, China), where the power and intensity of the NIR light were measured by an optical power meter (PM200, Thorlabs, Newton, NJ, USA). The Fe_3O_4/Au/PDA/PEI/FA/DOX NPs at various concentrations were placed in cuvette tubes, and NIR light was used to irradiate each sample. The distance between the sample and NIR light was set to 5 cm, and the light power was adjusted to 0.75 W cm^{-2}. Photothermal transduction photographs were obtained using a thermal camera (FLIR E60, Wilsonville, OR, USA) with a thermal sensitivity of 0.05 °C.

3. Results

3.1. Characterization of Fe_3O_4/Au NPs, Fe_3O_4/Au/PDA, and Fe_3O_4/Au/PDA/PEI/FA NPs

TEM was conducted to investigate the morphologies of Fe_3O_4/Au and Fe_3O_4/Au/PDA NPs. TEM image data revealed that the size of the Fe_3O_4/Au NPs was approximately 25–40 nm (figure 2(a)), where some aggregated or interconnected particles appeared. The TEM sample preparation process, particularly the air-drying procedure, may have led to the aggregation or interconnection of the NPs. In addition, energy-dispersive spectroscopy mapping (figure SI1 is available online at stacks.iop.org/NANO/28/425101/mmedia) indicated the elemental distributions of oxygen (green), iron (red), and gold (yellow). Figure 2(b) shows the TEM image of Fe_3O_4/Au/PDA NPs with an approximately 40 nm diameter, where a PDA shell approximately 4 nm thick was coated onto the surface of the Fe_3O_4/Au NPs after the self-polymerization of DA.

To assess the stability of the Fe_3O_4/Au/PDA and Fe_3O_4/Au/PDA/FA NPs in aqueous solution, we prepared them in 50% fetal bovine serum (FBS) buffer solution with the same density, and measured the size distributions after 1, 12, and 24 h of incubation [34] using dynamic light scattering (DLS). As to results, we could observe large aggregations of Fe_3O_4/Au/PDA NPs after 1 h incubation (figure SI 2(a), blue). Furthermore, Fe_3O_4/Au/PDA NPs showed superior stability and dispersion after 12 h (red) and 24 h (green) in the equivalent FBS buffer solution with average size of around 280 nm and narrow size distribution (figure SI 2(a)). The narrow size distribution indicates that the size of Fe_3O_4/Au/PDA NPs was maintained at around 280 nm and the NPs was stabilized after 12 h, though there was a spot of micro particles in the solution. Therefore, it is expected that the Fe_3O_4/Au/PDA NPs would have a good *in vivo* stability. Fe_3O_4/Au/PDA/FA NPs were assessed in the same condition, and an average size around 296 nm was observed, with narrow size distribution (figure SI 2(b)). In addition, it was observed that the size of Fe_3O_4/Au/PDA NPs obtained by TEM is smaller than NPs obtained by DLS. These results can be attributed to the fact that

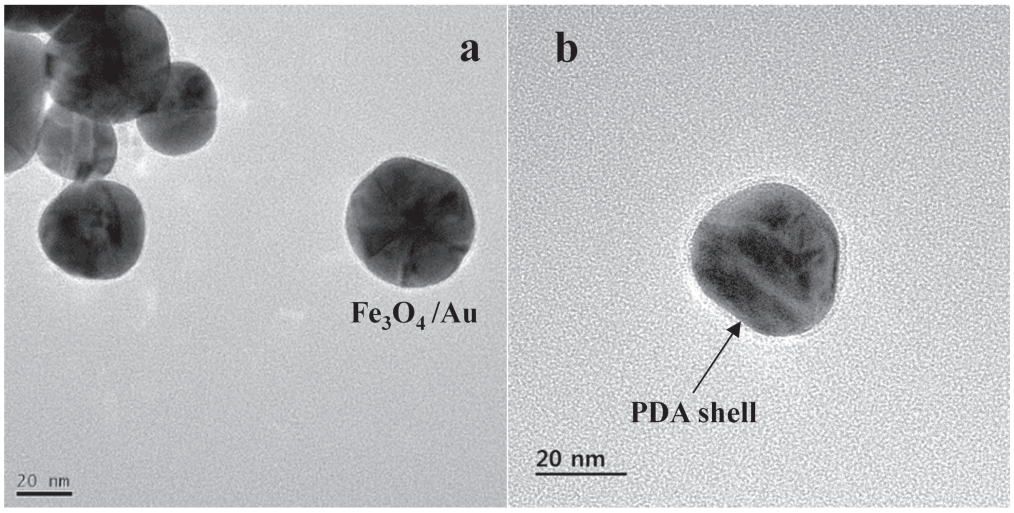

Figure 2. (a) TEM image of Fe_3O_4/Au NPs with sizes of 25–40 nm, and (b) TEM image of polydopamine (PDA)-coated Fe_3O_4/Au NPs with sizes of approximately 40 nm, where the thickness of the PDA shell was approximately 4 nm.

Fe_3O_4/Au/PDA NPs prepared for TEM observation were in a compact dry state, whereas those prepared for DLS were in a solvated state in which solvent molecules may interact with the Fe_3O_4/Au/PDA NPs, resulting in the increment of the size.

Zeta-potential, FT-IR, TGA, VSM, and XPS were evaluated to examine the intrinsic structures and properties of the Fe_3O_4/Au, Fe_3O_4/Au/PDA, and Fe_3O_4/Au/PDA/PEI/FA NPs (figures 3 and SI 4). As shown in figure 3(a), the zeta potential of Fe_3O_4 was −32.26 mV and after coating Au to the Fe_3O_4 core, and Fe_3O_4/Au NPs was approximately −28.2900 mV. After coating with PDA, the zeta potential of Fe_3O_4/Au/PDA was increased to −21.92 mV. Owing to the protonation of amine groups of PDA, the positively charged PDA successfully modified the surface charge of the Fe_3O_4/Au NPs. After PEI modification, the zeta potential of Fe_3O_4/Au/PDA was also increased to +20.89 mV due to protonation of the amine groups of PEI. Next, FA was conjugated with Fe_3O_4/Au/PDA NPs via an amide reaction between the amine groups of PEI and the carboxyl group of FA. After the conjugation of FA, the zeta potential of the Fe_3O_4/Au/PDA/PEI/FA NPs decreased slightly to +18.73 mV; FA may block the amine groups of PEI on the Fe_3O_4/Au/PDA NPs. Second, to confirm the conjugation of FA with Fe_3O_4/Au/PDA NPs, the FT-IR spectra of Fe_3O_4/Au, Fe_3O_4/Au/PDA, and Fe_3O_4/Au/PDA/PEI/FA are shown in figure 3(b). We observed a typical IR absorption peak for FA at 1608 cm^{-1} in the spectrum of Fe_3O_4/Au/PDA/PEI/FA, revealing that FA molecules were bound to Fe_3O_4/Au/PDA NPs [29]. Third, the composition of Fe_3O_4/Au/PDA/PEI/FA NPs was investigated by TGA (figure 3(c)).

The TGA curve of the Fe_3O_4/Au NPs revealed two main weight-loss steps; the first step occurred at 250 °C–350 °C because of water evaporation and the second step occurred at 350 °C–800 °C because of the metal core (Fe_3O_4/Au). In the TGA of Fe_3O_4/Au/PDA NPs, there were three weight-loss steps as follows: the first step (50 °C–280 °C) from water loss, the second step (280 °C–600 °C) from PDA loss, and the third step (600 °C–800 °C) from the metal core. The TGA curve of Fe_3O_4/Au/PDA/PEI/FA revealed three weight-loss steps: the first step (250 °C–420 °C) from water loss; the second step (420 °C–520 °C) from polymer loss including PDA, PEI, and FA; and the third step (520 °C–800 °C) from the metal core. Finally, because of the presence of the Fe_3O_4 core, Fe_3O_4/Au, Fe_3O_4/Au/PDA, and Fe_3O_4/Au/PDA/PEI/FA NPs showed superparamagnetism. The magnetizations of Fe_3O_4/Au, Fe_3O_4/Au/PDA, and Fe_3O_4/Au/PDA/PEI/FA NPs were measured by VSM. As shown in figure 3(d), via coating with PDA and conjugation of FA, the magnetization values per unit mass of Fe_3O_4/Au/PDA and Fe_3O_4/Au/PDA/PEI/FA NPs were decreased compared with that of Fe_3O_4/Au NPs. The magnetization curve shows that saturation magnetization (Ms) for Fe_3O_4/Au/PDA/PEI/FA (1.5 emu g^{-1}) and Fe_3O_4/Au/PDA (4.879 emu g^{-1}) was much smaller than that Fe_3O_4/Au (10.543 emu g^{-1}) at 300 K. The decrease in saturation magnetization was the result of the decrease of the effective mass of Fe_3O_4. The increased mass of the core–shell nanoparticle was introduced by the PDA shell. The superparamagnetic behavior of Fe_3O_4/Au/PDA mainly originated from the magnetic Fe_3O_4 core, while the PDA shell was nonmagnetic. In contrast to Fe_3O_4/Au, the 50% decrease in Ms of Fe_3O_4/Au/PDA could be attributed to the contribution of the diamagnetic PDA layer shell surrounding the magnetic Fe_3O_4 core [35, 36]. The value of the Fe_3O_4/Au/PDA/PEI/FA NPs' magnetization was reduced to 1.5 emu g^{-1} in a similar fashion.

The existence of elements on the surface of samples was studied by specific binding energy (eV) on x-ray photoelectron spectroscopy (XPS). This was employed as a useful method to acquire more quantitative data on the structure of the samples (figure SI 4). The surface elements of the core–shell nanoparticles (NPs) were identified according to the specific binding energy (eV) (figure SI 4(a)). To confirm the presence of Au on the surface of the Fe_3O_4 NPs, the Au element was specifically scanned. The peak of Au at 87.7 and

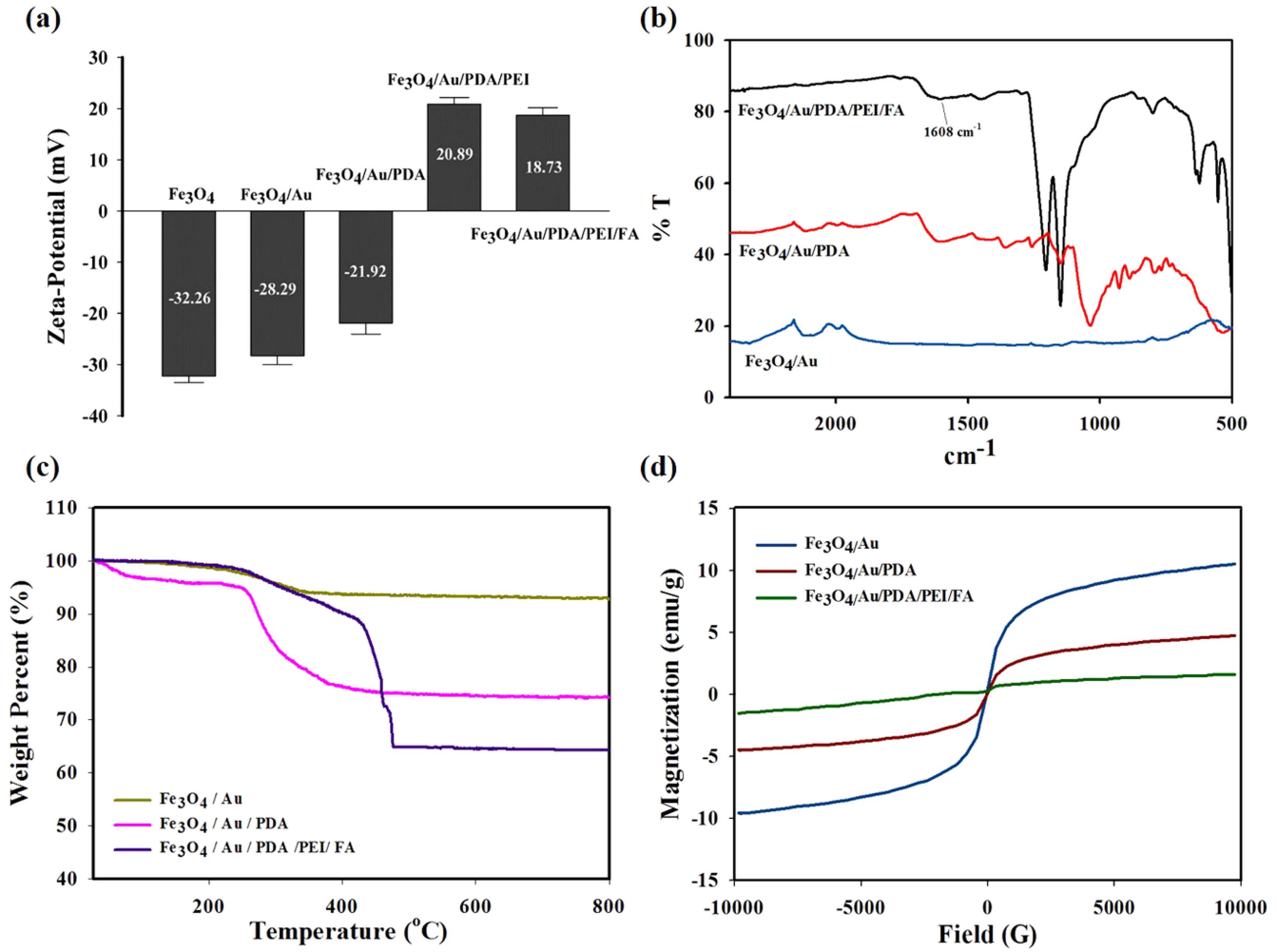

Figure 3. (a) Zeta potential of Fe_3O_4/Au, Fe_3O_4/Au/PDA, and Fe_3O_4/Au/PDA/PEI/FA in water; (b) FT-IR spectra of Fe_3O_4/Au, Fe_3O_4/Au/PDA, and Fe_3O_4/Au/PDA/PEI/FA; (c) TGA curves of Fe_3O_4/Au, Fe_3O_4/Au/PDA, and Fe_3O_4/Au/PDA/PEI/FA in nitrogen atmosphere (heating rate: 10 °C min^{-1}); and (d) VSM characterization.

84.1 eV is shown in figure SI 2(b) [37]. In figure SI 4(c), the PDA-coated NPs showed peaks at 399.6 and 285.04 eV, which are in response to nitrogen and carbon elements, verifying the presence of a PDA layer [38]. To prove the successful surface coating of PEI and FA on the PDA-coated NPs, nitrogen in the amino group on the Fe_3O_4/Au/PDA/PEI and Fe_3O_4/Au/PDA/PEI/FA NPs was specifically scanned because nitrogen and carbon exists in both the PEI and FA molecules. From figure SI 4(d), the distinct peak of signals from N1s and C1s verifies that PEI and FA coated the Fe_3O_4/Au/PDA NPs.

3.2. Photothermal effect using NIR light irradiation

An important feature of Fe_3O_4/Au/PDA/FA NPs is their NIR light-induced thermal effect for photothermal therapy. First, we measured the UV–vis-NIR absorbance spectrum (figure SI 3) with a multimode microplate reader (Thermo Fisher Scientific) to show the suitability of the evaluated temperature of the NPs using NIR laser. The results revealed that the Fe_3O_4/Au/PDA NPs exhibited a higher NIR absorbance than Fe_3O_4/Au NPs from 400–1000 nm due to the use of two photothermal agents, PDA and Au, together in a single nanoparticle system. Additionally, the Fe_3O_4/Au/PDA/FA NPs exhibited a slightly lower NIR absorbance than the Fe_3O_4/Au/PDA NPs because the folic acid coverage decreases the available nanoparticle surface to interact with light but still provides the required photothermal effect.

Second, to study the photothermal effect of NPs induced by NIR light irradiation, Fe_3O_4/Au/PDA NP sample solutions with different concentrations (0.005–0.1 ml ml^{-1}) were exposed to an NIR laser (808 nm, 0.75 W cm^{-2}) for 5 min and Fe_3O_4/Au and Fe_3O_4/Au/PDA/FA NPs solution at 0.1 mg ml^{-1} were irradiated with an NIR laser. As shown in figure 4(a), the temperatures of these Fe_3O_4/Au/PDA NP solutions increased during NIR irradiation. In addition, as the concentration of the Fe_3O_4/Au/PDA NPs increased, the temperature of the solutions increased. Moreover, the temperatures of the Fe_3O_4/Au/PDA and Fe_3O_4/Au/PDA/FA NP sample solutions with a concentration of 0.1 mg ml^{-1} were compared. The temperature of the Fe_3O_4/Au/PDA/FA solution increased from 26 °C–73 °C and the temperature of the Fe_3O_4/Au/PDA solution increased from 26 °C–77 °C, so there was only a slight difference between the two sample

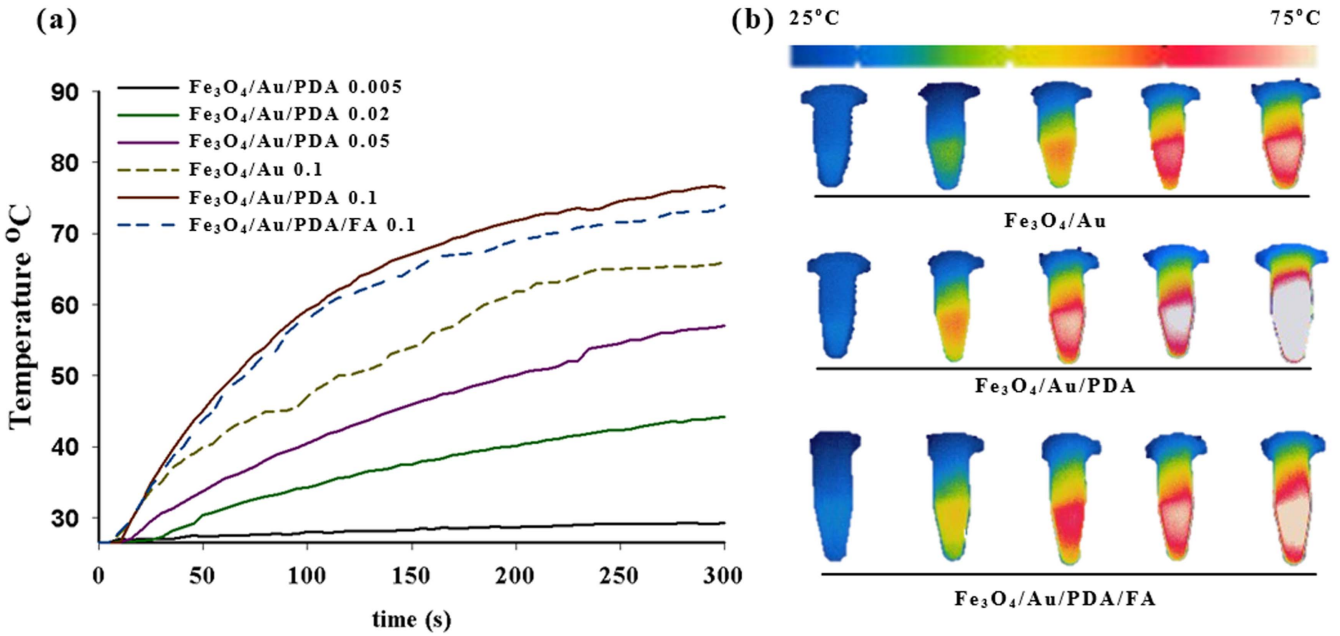

Figure 4. (a) Photothermal effect of NPs induced by NIR irradiation. Fe_3O_4/Au/PDA solutions of different concentrations (0.005–0.1 mg ml^{-1}) were exposed to an NIR laser (808 nm, 0.75 Wcm^{-2}, 5 min). In addition, Fe_3O_4/Au and Fe_3O_4/Au/PDA/FA solutions with a concentration of 0.1 mg ml^{-1} were exposed to the NIR laser under the same conditions. (b) NIR photothermal images of the Fe_3O_4/Au, Fe_3O_4/Au/PDA, and Fe_3O_4/Au/PDA/FA solutions at a concentration of 0.1 mg ml^{-1}.

solutions. In addition, figure 4(b) shows the NIR thermal images of the temperature of the Fe_3O_4/Au, Fe_3O_4/Au/PDA, and Fe_3O_4/Au/PDA/FA solutions at a concentration of 0.1 mg ml^{-1}. It was reported that cancer cells can be killed by incubation at 42 °C for 15–60 min and the duration can be shortened to 4–6 min when the temperature is greater than 50 °C [14]. These photothermal results indicate that Fe_3O_4/Au/PDA/FA NPs may be effective photothermal agents for cancer therapy.

3.3. Drug-releasing test

To test whether the photothermal effect of PDA enhanced DOX release from the NP solution, we performed controlled DOX release from Fe_3O_4/Au/PDA/FA/DOX NP solution combined with NIR light irradiation (figure SI 5) using the dialysis method. Two drug-release samples of Fe_3O_4/Au/PDA/FA/DOX NPs were prepared: one with and the other without NIR irradiation for 5 min at a power of 0.75 W cm^{-2} 12 h after the beginning of the experiment. The drug-release rate of Fe_3O_4/Au/PDA/FA/DOX NPs at 37 °C was very slow and the release rate was only 35% even 24 h later. In contrast, the drug-release rate rapidly increased by more than 56% after NIR irradiation, which is higher than the results reported in the current literature [11, 15, 20, 26, 39, 40]. The lower drug-release returned without NIR light irradiation. This result confirmed that NIR laser irradiation could be used to trigger drug release from the NPs, suggesting an approach to enabling on-demand drug release only to the target tissue so as to avoid damaging normal tissue. Fe_3O_4/Au/PDA/FA/DOX NPs may stably retain drugs under physiological conditions and, when locally heated up by external stimulus systems, drug liberation at the target regions will be enhanced. Thus, Fe_3O_4/Au/PDA/FA/DOX NPs combined with NIR light triggering can be used to control drug release.

3.4. Biocompatibility, cellular uptake, and cytotoxicity

The therapeutic efficacies of Fe_3O_4/Au/PDA/DOX and Fe_3O_4/Au/PDA/FA/DOX NPs were estimated by quantifying viability of 4T1 cells by MTT assay. As an important control experiment, the biocompatibilities of Fe_3O_4/Au/PDA and Fe_3O_4/Au/PDA/FA NPs were examined. As shown in figure SI 6, no significant cytotoxicity was observed even at a high concentration of 0.1 mg ml^{-1} NPs, indicating their good biocompatibility.

We evaluated the targeting and cell uptake of Fe_3O_4/Au/PDA/DOX and Fe_3O_4/Au/PDA/FA/DOX using CLSM, where DOX was used as a fluorescent probe and 4′,6-Diamidine-2′-phenylindole dihydrochloride (DAPI) was also used to identify the cellular nuclei. First, to confirm the targeting enhancement of NPs using the folate receptors, 4T1 cells were incubated with Fe_3O_4/Au/PDA/DOX and Fe_3O_4/Au/PDA/FA/DOX at the same DOX concentration (20 μg ml^{-1}) for 30 min at 37 °C. For competitive inhibition study, the cells were incubated with free FA (1 mg ml^{-1}) to block the folate receptors before the addition of Fe_3O_4/Au/PDA/FA/DOX. Next, the cells were carefully washed to remove free NPs and then re-incubated for 2 h before imaging by CLSM.

Cells treated with free DOX and untreated cells were selected as control groups (figure 5(a)). After washing with PBS to fully remove the free FA, Fe_3O_4/Au/PDA/DOX, and Fe_3O_4/Au/PDA/FA/DOX, confocal fluorescence images were acquired (figure 5(b)). From the DOX signal of the confocal images, Fe_3O_4/Au/PDA/FA/DOX showed enhanced

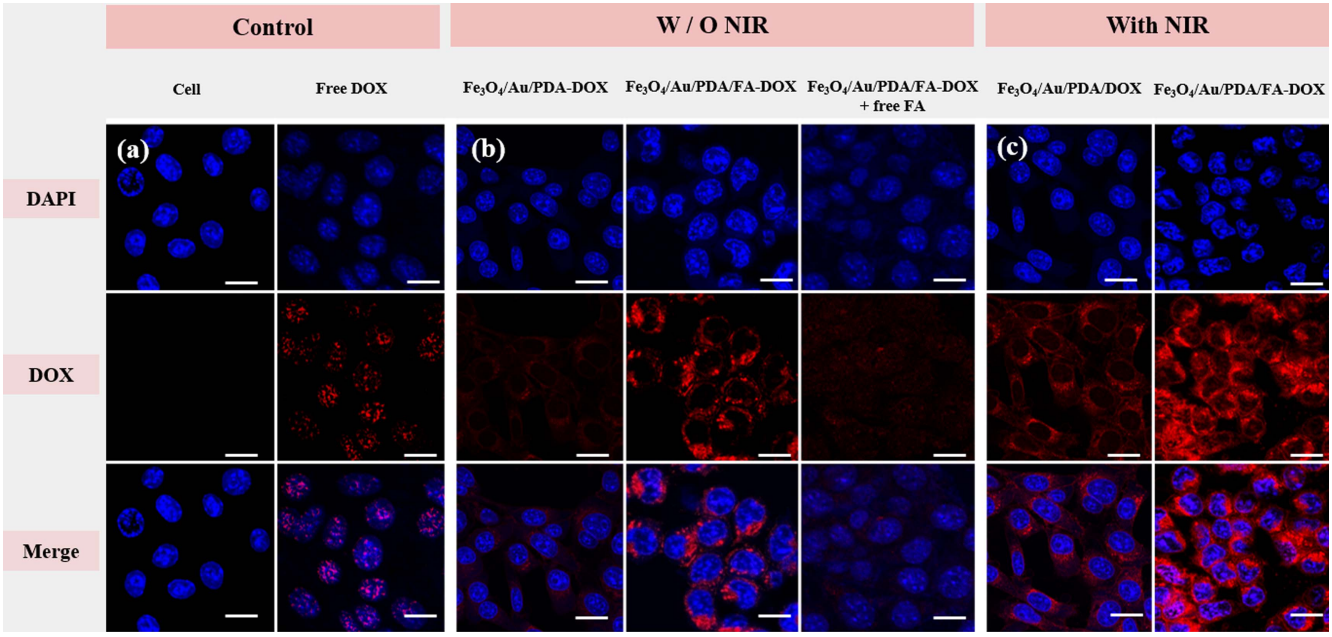

Figure 5. Effects on cellular uptake under folate receptor targeting and NIR irradiation. (a) 4T1 cells treated with free DOX and without any treatment as control groups. (b) 4T1 cells were treated with Fe_3O_4/Au/PDA/DOX and Fe_3O_4/Au/PDA/FA/DOX NPs, and another group of 4T1 cell was incubated with Fe_3O_4/Au/PDA/FA/DOX NPs after incubation with free FA (1 mg ml^{-1}) to block the folate receptors. (c) 4T1 cells were treated with Fe_3O_4/Au/PDA/DOX and Fe_3O_4/Au/PDA/FA/DOX NPs with NIR laser irradiation (808 nm, 0.75 W cm^{-2}) for 5 min (scale bar: 10 μm).

cellular uptake compared with Fe_3O_4/Au/PDA/DOX. Meanwhile, when folate receptors were blocked by free FA, much lower DOX intensity was observed.

Through irradiation with an NIR laser, we observed accelerated DOX release from Fe_3O_4/Au/PDA/FA/DOX NPs as shown in figure (SI 5). We evaluated the intracellular release behaviors of DOX from Fe_3O_4/Au/PDA/DOX and Fe_3O_4/Au/PDA/FA/DOX NPs in response to external NIR laser irradiation. To determine the NIR-triggered photothermal therapeutic efficiency, 4T1 cells and NPs were treated using the same procedure as in the previous cellular uptake test, and an NIR laser (808 nm, 750 mW.cm^{-2}) was irradiated for 5 min. The CLSM images (figure 5(c)) showed distinctly enhanced intracellular DOX fluorescence in Fe_3O_4/Au/PDA/DOX and Fe_3O_4/Au/PDA/FA/DOX NPs during NIR irradiation. Thus, NIR irradiation triggered the release of DOX from the internalized NPs inside the cells. In addition, as shown in figure 5(c), we found that the release of DOX from the Fe_3O_4/Au/PDA/FA/DOX was enhanced compared to Fe_3O_4/Au/PDA/DOX. This result demonstrates that NIR light irradiation enhanced DOX release from the internalized NPs inside the cells via FR-mediated endocytosis.

Finally, we evaluated whether the proposed NPs have an enhanced cancer-killing effect through FA targeting and NIR laser irradiation. 4T1 cells were incubated with free DOX, Fe_3O_4/Au/PDA/DOX, and Fe_3O_4/Au/PDA/FA/DOX with the same DOX concentration (20 μg ml^{-1}) for 30 min at 37 °C. Next, the 4T1 cells were carefully washed to remove free NPs and then re-incubated for 2 h. After washing with PBS to fully remove the free Fe_3O_4/Au/PDA/DOX and Fe_3O_4/Au/PDAFA/DOX NPs, 4T1 cells were treated with an NIR laser (808 nm, 750 mW.cm^{-2}) for 5 min. After further incubation for 24 h, the relative cell viabilities were measured by a standard cytotoxicity assay. As shown in figure 6, in the non-NIR-irradiated samples, the Fe_3O_4/Au/PDA/FA/DOX-treated cells (50% cell viability) showed more damage than the cells treated with Fe_3O_4/Au/PDA/DOX (64%) or free DOX (84%). After NIR laser irradiation, the Fe_3O_4/Au/PDA/FA/DOX-treated cells (18% cell viability) were more severely damaged than the cells treated with Fe_3O_4/Au/PDA/DOX (36%) and free DOX (82%) due to photothermal killing. Therefore, we found that tumor cells incubated with Fe_3O_4/Au/PDA/FA/DOX NPs showed the greatest cell death (~80%). These results also demonstrate that the proposed multifunctional NPs enhanced the cancer-killing effect via FA targeting and NIR laser irradiation.

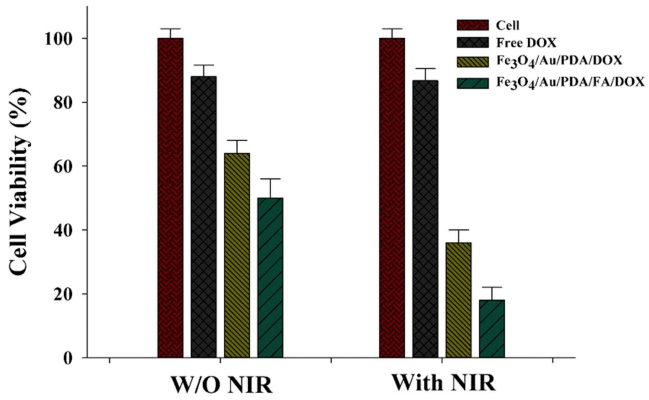

Figure 6. Cancer cell-killing effect of NPs, where 4T1 cells were incubated with free DOX, Fe_3O_4/Au/PDA/DOX, and Fe_3O_4/Au/PDA/FA/DOX NPs without (w/o) or with NIR laser irradiation (808 nm, 0.75 cm^{-2}, 5 min).

4. Discussion

In this study, we presented PDA-based NPs for FR-targeted and combined chemo-photothermal cancer therapy. First, we assessed the stability of the Fe_3O_4/Au /PDA and Fe_3O_4/Au/PDA/FA NPs in aqueous solution and measured their size distributions after 1, 12, and 24 h of incubation [34] using DLS. The proposed NPs showed progressively increased stability after 12 and 24 h in comparison with after 1 h incubation in 50% FBS buffer solution. We estimate that the proposed NPs have their surface charge (zeta potential values of Fe_3O_4/Au /PDA and Fe_3O_4/Au /PDA/FA NPs were about -21.92 and $+18.73$ mV, respectively, in aqueous environments) and may absorb some charged molecules or ions existing in the FBS solution. Further, we expect that the net charge of the NPs could be balanced by the formation of a cloud of counter-ions around the NPs. Therefore, the stability of the Fe_3O_4/Au /PDA or Fe_3O_4/Au /PDA/FA NPs could be lower in the first hour due to the balancing process of the net charge of the NPs. In addition, because there are some interactions between the molecules and ions, the NPs showed relatively wide size distribution in the first hour. However, as shown in figure SI 2, the size distribution of the NPs after 12 and 24 h was less narrow than that in the first hour. This suggests that the net charge of the NPs might be balanced and the NPs were stabilized after 12 and 24 h.S

Second, we expect that the proposed NPs could be used for photothermal therapy and/or MRI imaging. It has been reported that Fe_3O_4/gold core–shell structures not only endow NPs with unique magnetic and optical properties, but also ensure their biocompatibility [6, 8]. The proposed NPs have this Fe_3O_4/gold core–shell structure, as can be confirmed using the TEM image and EDS mapping. Furthermore, the magnetization value of the proposed NPs was 1.5 emu g^{-1} as measured by VSM. Meanwhile, it was reported that doxorubicin-loaded microbubbles with a magnetization value of only ± 0.015 emu g^{-1} could be used for concurrent MRI imaging [41]. Additionally, in another study, magnetic liposomes as *in situ* microbubble bombers, which had a size of about 200 nm and magnetization value of about ± 0.15 emu g^{-1}, were used for image-guided cancer theranostics [42]. Therefore, we expect that the proposed NPs, having a much higher magnetization value, can show superior performance in MRI imaging.

Third, PTT agents can be used alone or together to realize their therapeutic outcomes and various photothermal NPs, including noble metal and organic nanoagents such as Au NPs, carbon nanotubes, and PDA, have been extensively explored [43]. However, in the previous studies, they used high intensities (about 1–5 W cm^{-2}) of NIR irradiation, which could exceed the safe limit for cutaneous tissues (0.33 W cm^{-2}) [26]. Therefore, in this study, we employed a PDA/gold nanoparticle system and expected that the photothermal conversion rate of the proposed NPs, combined with two photothermal agents, would be higher than that of PDA or Au PTT agent alone. In addition, it was reported that a nanoparticle structure combined with two PTT agents could endow the NPs with not only the novel properties of the agents but also multifunctionality and unique applicability [6, 44, 45]. In our study, we validated and confirmed that the proposed PDA/gold nanoparticle has improved photothermal conversion rate due to the use of the two PTT agents. Although Fe_3O_4/Au/PDA/FA NPs exhibited a slight lower NIR absorbance than the Fe_3O_4/Au/PDA NPs because the folic acid coverage decreases the NP surface available to interact with light, the proposed nanoparticles still achieved the required photothermal effect.

Fourth, through a fundamental test, we validated that NIR laser irradiation at 0.75 W cm^{-2} for 5 min could trigger and enhance the controlled release of a loaded anti-tumor drug (DOX) in the proposed NPs. Consequently, we expect that NIR laser irradiation NIR is high enough to cleave the bond between the DOX and the rest of the iron/gold NP system.

Finally, the conjugation of folic acid using EDC reaction in the proposed NPs enhances the cancer-cell uptake efficiency via the folate receptor and thus improves chemotherapeutic efficiency. The higher cancer-cell targeting and uptake of the proposed NPs were also confirmed by CLSM.

Consequently, the proposed multifunctional NPs showed advanced photothermal and chemotherapeutic performance which was evaluated through *in vitro* experiments with a model cancer cell line. These results also demonstrate that the proposed NPs showed an enhanced cancer-killing effect via FA targeting and NIR laser irradiation.

5. Conclusion

In this paper, we propose FR-targeted, NIR-sensitive PDA-based NPs for chemo-photothermal cancer therapy. To fabricate the NPs, Fe_3O_4/Au was adopted as a metal core–shell NP with high magnetization value. PDA was coated by a self-polymerization method, FA was conjugated, and an anti-cancer drug (DOX) was loaded. The multifunctional NPs exhibited many advantages as a therapeutic drug-delivery system. First of all, the proposed NPs showed good biocompatibility and easy bioconjugation. The proposed NPs have an improved photothermal conversion ratio due to the combining of two photothermal agents (PDA and Au), and show an effective drug release and chemotherapeutic effect using low NIR intensity (0.75 W cm^{-2}). Because of the strong NIR absorption of Au/PDA, the proposed NPs can be effectively used for PTT by NIR laser irradiation. Through this NIR absorptivity, the proposed NPs can kill cancer cells directly via hyperthermia and can be used for the controlled release of the loaded DOX. In addition, NIR irradiation can promote the cell permeability of the NPs and improve their chemotherapeutic efficiency. Finally, through the conjugation of FA, the intracellular uptake and cell targeting of the proposed NPs were enhanced, and thus their chemotherapeutic efficiency was also increased. Consequently, based on the advantages of the proposed multifunctional NPs, we demonstrated effective chemo-photothermal cancer treatment through *in vitro* tests. We expect that the proposed

multifunctional NPs can be used as a drug-delivery system in cancer therapy.

Acknowledgments

This work was supported by the Ministry of Trade, Industry and Energy (MOTIE, Korea): Industrial Technology Innovation Program [10060059, Externally Actuatable Nanorobot System for Precise Targeting and Controlled Releasing of Drugs].

References

[1] Liu R, Guo Y, Odusote G, Qu F and Priestley R D 2013 *ACS Appl. Mater. Interfaces* **5** 9167–71
[2] Mezni A, Balti I, Mlayah A, Jouini N and Smiri L S 2013 *J. Phys. Chem.* C **117** 16166–74
[3] Seeta Rama Raju G, Benton L, Pavitra E and Yu J S 2015 *Chem. Commun. (Camb.)* **51** 13248–59
[4] Wang X *et al* 2013 *ACS Appl. Mater. Interfaces* **5** 4966–71
[5] Dong W, Li Y, Niu D, Ma Z, Gu J, Chen Y, Zhao W, Liu X, Liu C and Shi J 2011 *Adv. Mater.* **23** 5392–7
[6] Hu Y, Li J-C, Shen M-W and Shi X-Y 2014 *Chin. Phys.* B **23** 078704
[7] Jiang B, Wu Q, Deng N, Chen Y, Zhang L, Liang Z and Zhang Y 2016 *Nanoscale* **8** 4894–7
[8] Li J, Zheng L, Cai H, Sun W, Shen M, Zhang G and Shi X 2013 *ACS Appl. Mater. Interfaces* **5** 10357–66
[9] Li W-P, Liao P-Y, Su C-H and Yeh C-S 2014 *J. Am. Chem. Soc.* **136** 10062–75
[10] Cano M and de la Cueva-Mendez G 2015 *Chem. Commun.* **51** 3620–2
[11] Hervault A, Thanh N T K, Maenosono S, Lim M, Boyer C, Dunn A and Mott D M 2016 *Nanoscale* **8** 12152–61
[12] Lin J, Li Y, Li Y, Wu H, Yu F, Zhou S, Xie L, Luo F, Lin C and Hou Z 2015 *ACS Appl. Mater. Interfaces* **7** 11908–20
[13] Liu L, Zheng M, Librizzi D, Renette T, Merkel O M and Kissel T 2015 *Mol. Pharmaceut.* **13** 134–43
[14] Wang C, Xu H, Liang C, Liu Y, Li Z, Yang G, Cheng L, Li Y and Liu Z 2013 *ACS Nano* **7** 6782–95
[15] Darwish M S, El-Sabbagh A and Stibor I 2015 *J. Polym. Res.* **22** 1–6
[16] Ge J, Neofytou E, Cahill T J III, Beygui R E and Zare R N 2011 *ACS Nano* **6** 227–33
[17] Hayashi K, Nakamura M, Miki H, Ozaki S, Abe M, Matsumoto T, Sakamoto W, Yogo T and Ishimura K 2014 *Theranostics* **4** 834
[18] Schroeder A, Honen R, Turjeman K, Gabizon A, Kost J and Barenholz Y 2009 *J. Contr. Rel* **137** 63–8
[19] Troutman T S, Leung S J and Romanowski M 2009 *Adv. Mater.* **21** 2334–8
[20] Lin L-S, Cong Z-X, Cao J-B, Ke K-M, Peng Q-L, Gao J, Yang H-H, Liu G and Chen X 2014 *ACS Nano* **8** 3876–83
[21] Xiao Z, Ji C, Shi J, Pridgen E M, Frieder J, Wu J and Farokhzad O C 2012 *Angewandte Chemie* **124** 12023–7
[22] Huang X, Tang S, Mu X, Dai Y, Chen G, Zhou Z, Ruan F, Yang Z and Zheng N 2011 *Nat. Nano* **6** 28–32
[23] Kopwitthaya A, Yong K-T, Hu R, Roy I, Ding H, Vathy L A, Bergey E J and Prasad P N 2010 *Nanotechnology* **21** 315101
[24] Liu X, Tao H, Yang K, Zhang S, Lee S-T and Liu Z 2011 *Biomaterials* **32** 144–51
[25] Tian Q, Tang M, Sun Y, Zou R, Chen Z, Zhu M, Yang S, Wang J, Wang J and Hu J 2011 *Adv. Mater.* **23** 3542–7
[26] Espinosa A, Di Corato R, Kolosnjaj-Tabi J, Flaud P, Pellegrino T and Wilhelm C 2016 *ACS Nano* **10** 2436–46
[27] Liu Y, Ai K, Liu J, Deng M, He Y and Lu L 2013 *Adv. Mater.* **25** 1353–9
[28] Zhang R, Su S, Hu K, Shao L, Deng X, Sheng W and Wu Y 2015 *Nanoscale* **7** 19722–31
[29] Cheng F-F, Zhang J-J, Xu F, Hu L-H, Abdel-Halim E and Zhu J-J 2013 *J. Biomed. Nanotechnol* **9** 1155–63
[30] Scarano W, Duong H T, Lu H, De Souza P L and Stenzel M H 2013 *Biomacromolecules* **14** 962–75
[31] Herranz F, Salinas B, Groult H, Pellico J, Lechuga-Vieco A, Bhavesh R and Ruiz-Cabello J 2014 *Nanomaterials* **4** 408
[32] Zhou X, Xu W, Wang Y, Kuang Q, Shi Y, Zhong L and Zhang Q 2010 *J. Phys. Chem.* C **114** 19607–13
[33] Han J-W, Choi Y J, Cho S, Zheng S, Ko S Y, Park J-O and Park S 2016 *Sens. Actuat. B: Chemical* **224** 217–24
[34] Nguyen V D, Zheng S, Han J, Le V H, Park J-O and Park S 2017 *Colloids Surf. B: Biointerfaces* **154** 104–14
[35] Chen F, Chen Q, Fang S, Sun Y A, Chen Z, Xie G and Du Y 2011 *Dalton Trans.* **40** 10857–64
[36] Sun C, Lee J S and Zhang M 2008 *Adv. Drug. Deliv. Rev.* **60** 1252–65
[37] Tian Y, Chen L, Zhang J, Ma Z and Song C 2012 *J. Nanopart. Res.* **14** 1–11
[38] Park J, Brust T F, Lee H J, Lee S C, Watts V J and Yeo Y 2014 *ACS Nano* **8** 3347–56
[39] Wang C, Wang X, Zhong T, Zhao Y, Zhang W-Q, Ren W, Huang D, Zhang S, Guo Y and Yao X 2015 *Int. J. Nanomed* **10** 2229
[40] Ling D, Park W, Park S-J, Lu Y, Kim K S, Hackett M J, Kim B H, Yim H, Jeon Y S and Na K 2014 *J. Am. Chem. Soc.* **136** 5647–55
[41] Fan C-H, Ting C-Y, Lin H-J, Wang C-H, Liu H-L, Yen T-C and Yeh C-K 2013 *Biomaterials* **34** 3706–15
[42] Liu Y *et al* 2017 *ACS Nano* **11** 1509–19
[43] Zou L, Wang H, He B, Zeng L, Tan T, Cao H, He X, Zhang Z, Guo S and Li Y 2016 *Theranostics* **6** 762
[44] Wang Y, Shen Y, Xie A, Li S, Wang X and Cai Y 2010 *J. Phys. Chem.* C **114** 4297–301
[45] Lou L, Yu K, Zhang Z, Huang R, Zhu J, Wang Y and Zhu Z 2012 *Nano Res.* **5** 272–82